J. Cell. Mol. Med. Vol 16, No 12, 2012 pp. 3037-3051

Metastasis-associated gene, *mag-1* improves tumour microenvironmental adaptation and potentiates tumour metastasis

Yan Wang [a, #, *], Haiquan Jia [b, #], Huiyun Lin [b, #], Xiaogang Tan [b], Zhiyan Du [a], Huihua Chen [b], Yuanji Xu [b], Xiaoxi Han [b], Jiakai Zhang [a], Siyang Zhao [a], Xiaodan Yu [b], Yinglin Lu [a, b, *]

[a] *Department of Advanced Interdisciplinary Studies, Institute of Basic Medical Sciences, Beijing, China*
[b] *Department of Pathobiology, Institute of Basic Medical Sciences, Beijing, China*

Received: January 31, 2012; Accepted: September 3, 2012

Abstract

Metastasis is a major cause of death from malignant diseases, and the underlying mechanisms are still largely not known. A detailed probe into the factors which may regulate tumour invasion and metastasis contributes to novel anti-metastatic therapies. We previously identified a novel metastasis-associated gene 1 (*mag-1*) by means of metastatic phenotype cloning. Then we characterized the gene expression profile of *mag-1* and showed that it promoted cell migration, adhesion and invasion *in vitro*. Importantly, the disruption of *mag-1 via* RNA interference not only inhibited cellular metastatic behaviours but also significantly reduced tumour weight and restrained mouse breast cancer cells to metastasize to lungs in spontaneous metastatic assay *in vivo*. Furthermore, we proved that *mag-1* integrates dual regulating mechanisms through the stabilization of HIF-1α and the activation of mTOR signalling pathway. We also found that *mag-1*-induced metastatic promotion could be abrogated by mTOR specific inhibitor, rapamycin. Taken together, the findings identified a direct role that *mag-1* played in metastasis and implicated its function in cellular adaptation to tumour microenvironment.

Keywords: metastasis-associated gene • tumour microenvironment • HIF-1α • mTOR signalling pathway • tumour metastasis

Introduction

Cancer metastasis depends on a complex and dynamic microenvironment where tumours and their metastases develop and seed [1, 2]. The tumour microenvironment, which is characterized by regions of hypoxia, low nutrition and acidosis because of defective vasculature has been recognized as a major factor to influence tumour cell behaviours [3, 4]. Solid malignancies typically require an increasing accommodation to microenvironment for their constant growth and metastasis [5]. This in turn has aroused the current extensive interest in the critical molecules related to adaptive responses in the tumour microenvironment, which will be treated as potential molecular target for cancer therapy.

Hypoxia is now considered as a fundamentally important characteristic of the tumour microenvironment. The hypoxia-inducible factor 1 (HIF-1) is the primary regulator of the cellular response to hypoxia [6]. It is a heterodimeric factor composed of an oxygen-regulated HIF-1α subunit and a constitutive HIF-1β/ARNT (aryl hydrocarbon receptor nuclear translocator) subunit [7], and its transcriptional activity is largely determined by regulated expression of the HIF-1α subunit [8]. Under normoxia, HIF-1α protein level is precisely regulated by hydroxylation and ubiquitin-proteasomal degradation in an oxygen-dependent manner, whereas hypoxia signalling stabilizes HIF-1α by inhibiting the above-mentioned pathway [9]. Then, HIF-1α rapidly accumulates, translocates into the nucleus and dimerizes with HIF-1β/ARNT, binding to the hypoxia-responsive DNA element, recruiting the transcriptional coactivator p300/CBP for transcriptional induction of a host of hypoxia-responsive genes involved notably in glycolysis and angiogenesis [10, 11], and allowing cells to adapt to hypoxia [12]. HIF-1α is found to overexpress frequently in human cancers and its increment has proven to be correlated with poor patient prognosis [13, 14]. Numerous researches have shown that HIF-1α-mediated gene transcriptional

#These authors contributed equally to this work.
*Correspondence to: Ying-Lin Lu or Yan Wang, Department of Advanced Interdisciplinary Studies, Institute of Basic Medical Sciences, 27 Taiping Road, Beijing 100850, China.
Tel.: +8610-68166874
Fax: +8610-68166874
E-mails: luyinglin@hotmail.com, yan_way@yahoo.com.cn

doi: 10.1111/j.1582-4934.2012.01633.x

regulation is a positive factor in tumour metastasis including neovascularization, cell survival, glucose metabolism, invasion and especially metastasis [15–17].

Additional oxygen sensitive signalling pathways including mammalian target of rapamycin (mTOR) pathway also contribute to the cellular adaptation to the tumour microenvironment [18]. mTOR pathway is a downstream effector of the phosphatidilinositol-3 kinase (PI3K)/Akt pathway, which regulates cell proliferation and viability. Deregulations in mTOR signalling are frequently associated with tumorigenesis, angiogenesis and tumour growth. Recent studies show that mTOR also plays a critical role in the regulation of tumour cell motility, invasion and cancer metastasis [19, 20]. The mitogenic stimulators of insulin, nutrients and growth factors activate PI3K/Akt cascade, which inactivates the TSC1/TSC2 inhibitor complexes and relieves mTOR from inhibition, induce mTOR activation. mTORC1 phosphorylates p70 S6 kinase (S6K1) and eukaryotic initiation factor 4E (eIF4E) binding protein 1 (4E-BP1) assist ribosome biogenesis, transcription and cap-dependent translation [21–23]. mTORC2 phosphorylates Akt, protein kinase C alpha (PKC alpha) and the focal adhesion proteins, control the activities of the small GTPases (RhoA, Cdc42 and Rac1), and regulate cell survival, actin cytoskeleton assembly and motility. As PI3K-mTOR pathway links to oncogenic signalling and is deregulated in approximately 50% of all human malignancies, mTOR signalling is a major anti-cancer drug target with potential therapeutic value [24–26].

We previously adopted phenotype cloning methods to identify a novel metastasis-associated gene 1 (*mag-1*) which is closely related to the metastatic phenotypes of lung cancer *in vitro* and to the metastatic potential in clinical cancer tissues [27, 28]. This sequence was submitted to GenBank and was named as *mag-1*. We searched public databases and found that it shares significant similarity with MGC11324 (GenBank accession no. NM_032717) [29]. This cDNA has an acetyl transferase motif, and later, it was identified subsequently as one of the phospholipids enzyme isoforms participating in the lipid biosynthesis. Tang *et al.* identified this sequence as a novel human lysophosphatidic acid acyltransferase family member, LPAAT θ [30]. However, they did not clarify its enzymatic activity and specific function. Other groups isolated the same sequence predicted from different acyltransferase families and identified its distinct enzymatic activities. Cao *et al.* reported a same protein sequence labelled as GPAT3 with a significant NEM-sensitive GPAT activity, instead of the expected lysophosphatidic acid acyltransferase activity or acyltransferase activities against a variety of other substrates [31–33]. Sukumaran *et al.* determined that the same isoform has only a robust AGPAT activity in human embryonic kidney 293 cells infected with recombinant GPAT3 adenovirus and they named it as AGPAT10 [34]. Despite the discrepancy of its enzymatic activities, the protein has been demonstrated as an important acyltransferase enzyme in lipogenesis. However, whether this cDNA sequence functions in tumour progression or not is not estimated yet.

Here, we identified the gene expression profile of *mag-1* as well as its subcellular localization. Through metastatic phenotypic analysis, we validated the significant association of *mag-1* with tumour metastasis both *in vivo* and *in vitro*. *mag-1* was proven to be a potential regulator of HIF-1α *via* activating mTOR signalling pathway. Moreover, we also observed that *mag-1*- mediated mTOR activation is of great importance for tumour metastatic phenotypes. These findings shed light on the mechanisms by which *mag-1* potentiates cancer cell to metastasize through their metabolic adaptation to tumour microenvironment.

Materials and methods

Additional details of materials and methods can be found in Supplementary Information.

Plasmid constructs

The complete open reading frame of *mag-1* (GenBank, NM_032717) was cloned into a mammalian expression vector pcDNA3.1/Myc-HisA$^+$. For RNA interference assay, three short interfering RNA (siRNA) template oligonucleotides targeted to *mag-1* were designed and cloned intopSilencer 2.1_U6 (Ambion, Austin, TX, USA; hereafter abbreviated to pSilencer). The targeted site and sequences are as follows: 304 AAGGGATTGGAAGCCATTGTA; 877 AAGAAGAAACTACCCAT ACTA; 908 AAGGAACTTGCATCAACAATA. A plasmid encoding a hairpin siRNA whose sequence did not match any known human coding cDNA was applied as a negative control. The recombinant plasmids were confirmed by sequencing analysis.

Cell culture

Cells were cultured and maintained in RPMI1640 or DMEM media supplemented with 10% FBS under standard conditions (37°C, 5% CO_2). For transfection, 70–80% confluent cells in six-well plastic plates were transfected with the appropriate plasmids using Mega Trans 1.0 (Origene, Rockville, MD, USA) in accordance with the manufacturer's protocol. For stable expression, the transfected cells were passaged at a 1:10 dilution and screened with G418 (700 μg/ml) for about 3 weeks. The stable clones were obtained and expanded for further experiments.

Northern blot analysis

Total RNA (50 μg) was fractionated by electrophoresis on 1% agarose gel plates containing formaldehyde and transferred to nitrocellulose membrane, and the membranes were baked at 80°C, for 2 hrs. For gene profile assay, a human tumour tissue Northern blot (MTN) and a human multiple tissue expression array (BD^{TM}MTE) (BD Clontech, Mountain View, CA, USA) were pre-made with Poly (A)$^+$ RNA. The membranes were hybridized to the specific probes generated with the Klenow fragment of DNA polymerase I and [α-^{32}P]-dCTP by using Prime-a-Gene® Labeling System (Promega, Madison, WI, USA). The hybridization was carried out as instructed by the manufacturer. β-actin and ubiquitin cDNA were, respectively, applied as control. The membranes were then exposed to an X-ray film at −70°C with an intensifying screen. The spots or bands on the exposed film were scanned and analysed under Tanon GIS gel imaging system (Bio-Tanon Co., Ltd., Shanghai, China).

Animals and *in vivo* spontaneous metastasis assay

The recipients were adult female BALB/c mice (6–8 weeks). All animals were provided and all experiments were approved by the Experimental Animal Center of the Beijing Institute of Basic Medical Sciences. EMT6/*mag-1* KD, mock control and scramble-shRNA control (non-silencer) cells were, respectively, inoculated to the mammary fat pad of female BALB/c mice. The mice were killed when tumours reached a mean volume of 8 cm^3 and they exhibited a symptom of cachexia. At necropsy, the tumours were harvested from the mice and the tumour mass weights were measured. The gross metastatic nodules were observed and photographed under anatomical microscopy. For histological analysis, the lungs and mammary tumour tissues were embedded in paraffin and the sections were cut and stained with haematoxylin-eosin. The metastases in the total lungs were counted and metastatic frequency was analysed. Whole mounts were digitally photographed under a microscope under the same magnification and light conditions for all samples.

Hypoxia experiment

The hypoxia system was established according to previously published procedure [35]. For the treatment with short-term hypoxia, cells were incubated in a hypoxia chamber maintaining 0.5% O_2 for 6–24 hrs. The cell lysis was prepared on ice instantly after the hypoxia treatment to avoid the reoxygenation-induced polyubiquitination and degradation of HIF-1α. For the analysis of the half-life of HIF-1α, stably transfected H1299 cells and mock control cells were incubated in hypoxia for 8 hrs and then treated with 25 mg/l cycloheximide, after which the decay of HIF-1α was monitored at the indicated time using Western blot.

Cell adhesion assay

Each well in 96-well tissue culture plates was coated with 2 μg of Matrigel (RD, Bedford, MA, USA) incubated overnight at 4°C. The wells were washed three times with PBS to remove excess, and the unbound Matrigel was blocked with 100 μl of a 10% bovine serum albumin (BSA; Sigma-Aldrich, St. Louis, MO, USA) solution in RPMI1640 medium for 1 hr at 37°C. Aliquots of 2×10^4 cells in 100 μl of serum-free RPMI1640 medium were added to each well and the cells were allowed to adhere for 1 hr at 37°C. Then, the numbers of adhering cells were counted by MTT assay. Results were expressed as the adhesive rate (%) calculated according to the following formula: (OD value of the adhered cells/OD value of total cells) $\times$100%.

Transwell cell invasion assay

The migration and invasion of cells was assayed in transwell chambers with 6.5-mm-diameter polycarbonate membrane filters containing 8 μm pores (Corning Costar, Corning, NY, USA). Fibroblast-conditioned medium, which was obtained from confluent NIH3T3 cell cultures in serum-free RPMI 1640 was used as the chemotactic attractant and added to the 24-well companion plate. For the invasion assay, transwell insert was coated with 120 μg basement membrane Matrigel per filter. 1×10^5 cells were plated in the transwell insert and then incubated at 37°C. After 24 hrs, the non-migrating cells and the Matrigel in the upper surface of the membrane were removed with a cotton swab. The filters were fixed in paraformaldehyde and stained with H.E. Three random visual fields (40$\times$) on the lower surface of the membrane were selected to count cells penetrating the membrane. Migrant ability was denoted as the average number of penetrating cells. Each assay was performed thrice in triplicate.

Wound healing cell migration assay

Cells were plated at the density of 7×10^5 cells per well on a 6-well plate in normal culture medium and allowed to reach 100% confluence. The injury line was made with a sterile pipette tip of 2 mm in width and then cells were rinsed with PBS and incubated for 20 hrs. The cell-free area was selected, measured and quantified by using the UTHSCSA ImageTool 3.0 software (an image processing and analysis programmed by the researcher of the University of Texas Health Science Center at San Antonio) and calculated as a percentage of wound healing according to the equation: wound healing (%) = [1 – (wound area at T20 hrs/wound area at T0)] $\times$ 100%, where the T20 is the detected time-point and T0 is the time immediately after wounding.

Luciferase reporter assay

The HRE-luciferase reporter plasmid was a gift from EE Voest (University Medical Center Utrecht, The Netherlands). It contains wild-type HRE oligonucleotide of the 3′-enhancer of the human erythropoietin gene in triplicate in front of a minimal TK promoter [36] in the pBlLuc vector backbone. Assays were performed under the instruction of the Dual-Glo luciferase assay system (Promega).

Immunofluorescent staining

The cells grown on the 35 mm glass bottom of the microwell cell culture dishes (MatTek corporation, Ikitelli, Istanbul, Turkey) were fixed in 4% paraformaldehyde for 15 min., followed by permeabilization in 0.2% Triton X-100 for 15 min. After 1 hr blocking in PBS with 3% BSA and 5% newborn calf serum, the samples were incubated overnight in the primary antibody diluted in blocking solution. Subsequently, the samples were stained with the second antibodies and double stained with 1 μg/ml Hoechst 33258. All cell samples were visualized using Confocal laser- scanning microscope (Zeiss 510 META, Oberkochen, Germany).

Semi-quantitative RT-PCR and quantitative real time PCR (qRT-PCR)

Methods used for RNA isolation, purification and reverse transcription were performed under the instructions of the manufacturers (Invitrogen, Grand Island, NY, USA). qRT-PCR was performed by using Mx3000 comparative quantitation systems (Stratagene, La Jolla, CA, USA) with a standard temperature protocol and 2$\times$SYBR Green PCR Master Mix reagent (CW Biotechnologies, Beijing, China) in a 20 μl volume in triplicate. As a control, the mRNA level of GAPDH was determined in the real time PCR assay for each RNA sample and was

used to correct experimental variations. The primer sequences were used as follows: VEGF primers: Forward 5′- ATGAACTTTCTGCTGTC TTG-3′ Reverse 5′-TGAACTTCACCACTTCGT-3′, *mag-1* primers: Forward 5′-GAAGATGCAGTC CAGTTTGCT-3′ Reverse 5′-TGAAGAAAGTGGCAAG GCTA-3′, GAPDH (as control) primers: Forward 5′-ACC ACAGTCCATGC CATCAC-3′ Reverse 5′-TCCACCACC CTGTTGCTGTA-3′.

Statistical analysis

All the data were presented as means ± S.D. One-way ANOVA with non-parametric analysis was performed using GraphPad Prism version 5.00 for Windows, GraphPad Software (San Diego, California, USA, www.graphpad.com). $P < 0.05$ was regarded statistically significant ($*P < 0.05$; $**P < 0.01$; $***P < 0.001$).

Results

mag-1 gene expression profiles are associated with tumour metastatic phenotype

To confirm whether or not *mag-1* is related to the formation of cancer as well as its metastasis, we firstly validated the differential expression of *mag-1* between poorly and highly metastatic human lung giant cell carcinoma sublines, PLA801C and PLA801D [37]. Semiquantitative RT-PCR and northern blot analysis clearly indicated that *mag-1* expressed sixfold to eightfold higher in PLA801D than that in PLA801C cells (Fig. 1A). Concomitantly, the protein levels displayed about fourfold to fivefold difference between these two cells in Western blot analysis.

To identify *mag-1* gene, we evaluated the molecular size and the distribution of Mag-1 protein within cells. In Figure 1B, the molecular weight of Mag-1 was clearly indicated as 43 kD. Furthermore, we determined the subcelluar localization of Mag-1. In COS-7 and H1299 cells stably expressing the Mag-1-His fusion protein, fluorescence confocal images showed an endoplasmic reticulum (ER)-like expression pattern. This subcellular localization was confirmed by co-localizing Mag-1-His with the ER-specific protein Calnexin (Fig. 1C). Meanwhile, the membrane and cytoplasmic fractions which were separated from these two cell lines were subjected to Western blot assay. It was clearly indicated that Mag-1 and Calnexin mainly co-localized in membrane fraction, especially in ER (Fig. 1D). As GPAT3, AGPAT10 and LPAAT θ have been reported to localize in ER or microsome, Mag-1 shares the same subcellular compartment with these enzymes [30, 33, 34].

Northern blot analysis of *mag-1* expression in eight human tumour tissues revealed one transcript of about 2.2 kb and an additional transcript of 3.5 kb exclusively in the ovary tumour. *mag-1* expressed highly in uterus, kidney, breast, ovary and stomach tumours, but moderately in lung, rectum and colon tumours (Fig. 1E). In addition, there appeared a variation of Mag-1 protein level in multiple cancer cell lines. Concomitant to the result observed in PLA801C and D, the other pair of human lung giant cell carcinoma sublines with different metastatic capacity—PG (poorly metastatic) and BE1 (highly metastatic) strains (with the same origin of PLA801C and D) —also exhibited variant expressions of *mag-1*. Its expression in BE1 was higher than that in PG cells. A weak band was detected in human non-small cell lung carcinoma cell lines (NSCLC) A549 and H1299, whereas a strong one in H322, H2087 and H596 cell lines. Finally, Mag-1 expression was shown higher in HL-60 (human leukaemia cell line), SKOV3 (human ovarian carcinoma cell line) and CNE-2 (human nasopharyngeal carcinoma cell line) than that in MCF-7 (human breast carcinoma cell line), Hela (Human cervical carcinoma cell line), HepG2, Bel7402, SMMC7721 (Human liver carcinoma cell lines) and K562 cells (human leukaemia cell line) (Fig. 1F). With our former findings that *mag-1* transcription correlates with metastatic potential in clinical tumour samples, these data could give a cogent support to such the conclusion that the expression of *mag-1* gene has a positive interconnection with tumour metastasis.

mag-1 promotes tumour cell metastatic phenotypes *in vitro*

To characterize the function of *mag-1* in cell biological behaviours involving in metastasis, we overexpressed *mag-1* in poorly metastatic cell, PLA801C by gene transfection, and selected the stably transfected cell strains. We observed that the overexpression of *mag-1* moderately augmented the adhesion of PLA801C cells to Matrigel (Fig. 2A). The wound healing migration assay showed that PLA801C/*mag-1* exhibited much higher healing rate than mock control cells during the follow-up period 20 hrs after injury (Fig. 2B). This result suggested that *mag-1* accelerates cell mobility. Moreover, *mag-1* overexpression enhanced PLA801C cells invasion through artificial basement membrane, Matrigel-coated transwells twofold over mock controls (Fig. 2C).

To evaluate the effects of *mag-1*-silencing on cell metastatic phenotypes, we knocked down the expression of endogenous *mag-1* in PLA801D by using specific *mag-1* shRNA. As is shown in Figure 2D, *mag-1* expression levels were reduced in PLA801D/*mag-1* KD cells. Subsequently, the cell adhesion assay revealed that the disruption of *mag-1* resulted in the decreased cell adhesion to artificial basement membrane, Matrigel. The cell migration rate of PLA801D/*mag-1* KD cells declined to 38.7% compared to 47.5% of PLA801D/control cells in wound healing assay (Fig. 2E). Furthermore, the cells invaded through transwell membrane were also reduced by *mag-1* knockdown (Fig. 2F). As cell migration, adhesion and invasion abilities are the essential characteristics of malignant tumour cells, the above reciprocal assessment indicated that *mag-1* accelerates tumour metastasis *in vitro*.

mag-1 is required for tumour metastasis *in vivo*

To determine the roles of native *mag-1* in tumour metastasis *in vivo*, we established *mag-1* stably knock-down mouse breast cancer EMT6 cell by means of RNA interference. The efficient *mag-1* KD cell clones

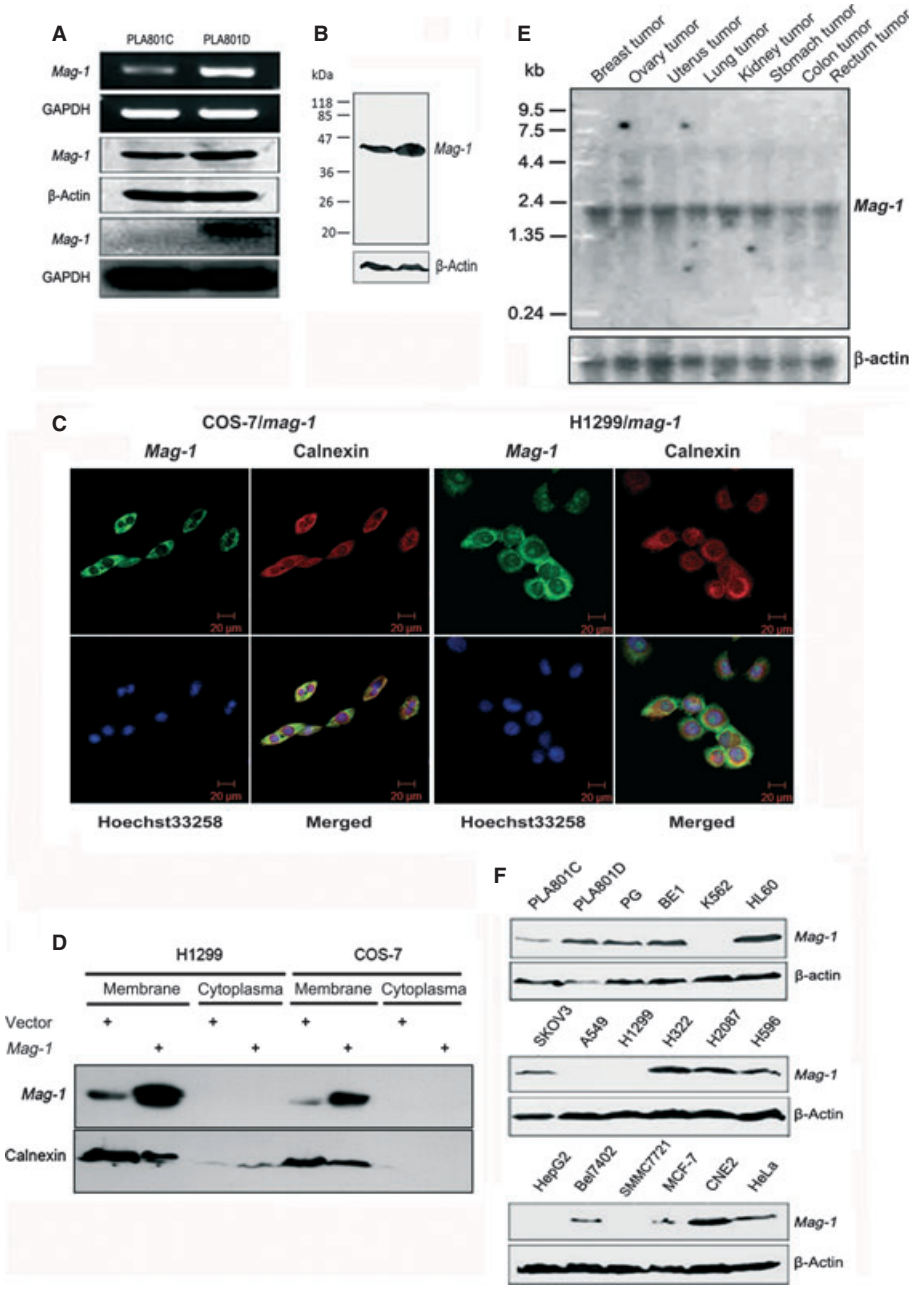

Fig. 1 Identification and expression profile of *mag-1* gene. (**A**) Verification of differential expression of *mag-1* in PLA801C and D cells. Upper two lines indicate semi-quantitative RT-PCR analysis of *mag-1* mRNAs. Middle two lines are Western blot analysis of Mag-1 protein levels using β-actin as internal control between PLA801C and D. Lower two lines indicate northern blot analysis of *mag-1* mRNAs using GAPDH as internal control between PLA801C and PLA801D. (**B**) Molecular weight of Mag-1 protein analysed using Western blot analysis. (**C**) Subcellular localization of Mag-1 within cells. A immunofluorescent staining of COS-7 and H1299 cells overexpressing His-Tagged Mag-1. Mag-1 was stained with anti-His antibody (Green) and visualized co-localization with ER specific protein, Calnexin (Red). Cells were double stained with Hoechst 33258 (blue) to identify the nuclei in the corresponding fields. All cell samples were visualized using Confocal laser-scanning microscope (Zeiss 510 META, Oberkochen, Germany). (**D**) Western blot analysis of cell membrane and cytoplasma fraction from H1299 and COS-7 cells, stably transfected *mag-1* or vector control. (**E**) Northern blot analysis of *mag-1* transcription in eight human tissues. A human multiple tissue northern blot membrane was hybridized with ^{32}P-labelled *mag-1* specific or β-actin cDNA probes (bottom) respectively. Hybridization with β-actin served as a loading control. Size marker is indicated on the left. (**F**) Western blot analysis of *mag-1* protein in multiple cancer cell lines. β-Actin was used as an internal control.

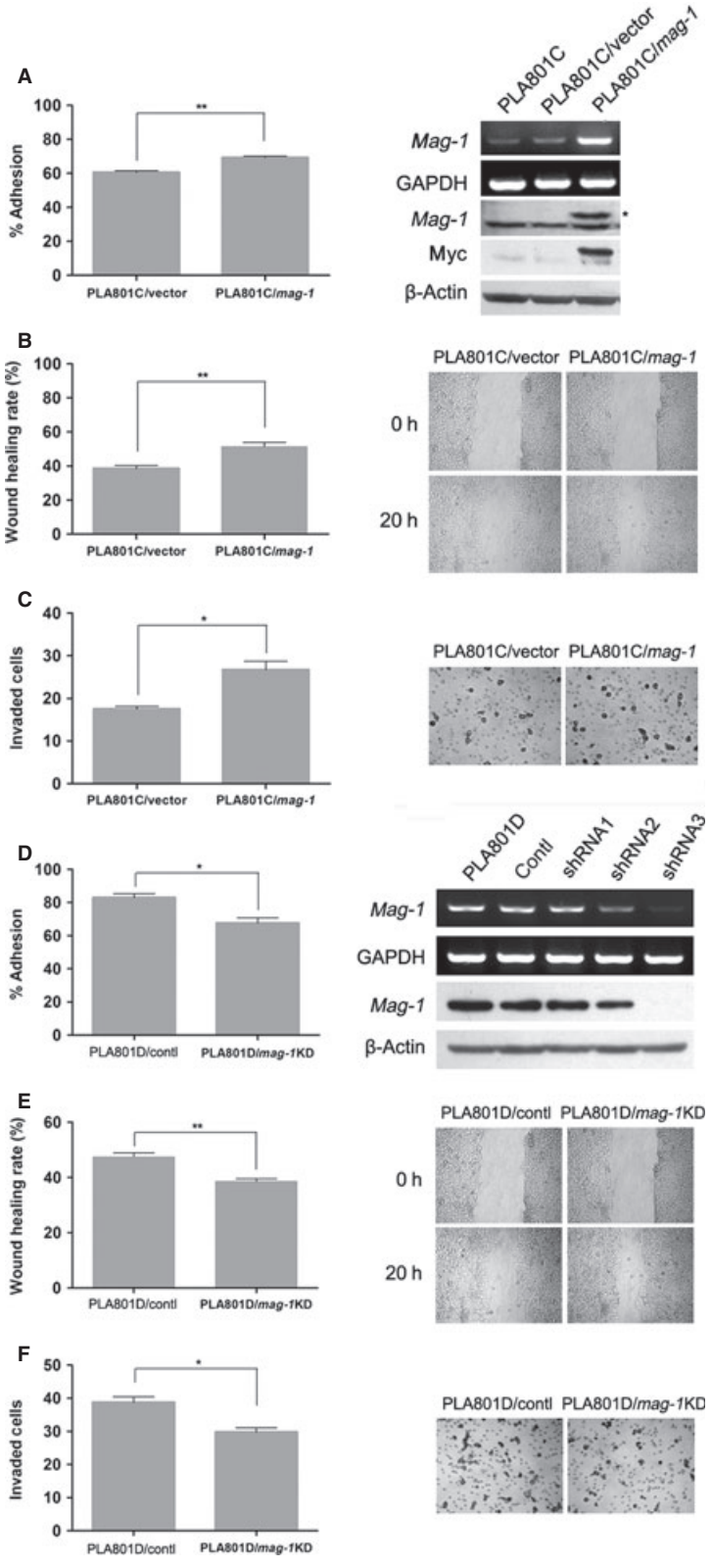

Fig. 2 Effect of *mag-1* on cell adhesion, migration and invasion capability of human lung cancer cells *in vitro*. (**A**) Adhesion of PLA801C/*mag-1* and mock control cells to Matrigel. The cells were added to each 96-well coated with Matrigel. After 1 hr of incubation, tumour cell adhesion was measured using MTT assay. Results were shown as the adhesion rate calculated according to the formula: (A490 nm of the adhered cells/A490 nm of total cells)×100%. The exogenous *mag-1* expression was analysed by RT-PCR (upper two lines) and Western blot assay (middle two lines). Arrow indicates myc-tagged Mag-1 protein. (**B**) Cell migration after injury. A total of 7×10^5 cells per well were seeded on a 6-well plate in normal culture medium and allowed to reach 100% confluence. The injury line was introduced to scratch the cell monolayer with a sterile pipette tip of 2 mm in width, and then cells were rinsed with PBS and incubated for 20 hrs. Wound closure was monitored by visual examination using an Olympus microscope. (**C**) Transwell cell invasion assay. 1×10^5 cells were plated in the upper layer of each transwell (coated with 120 μg basement membrane, Matrigel) and then, incubated at 37°C for 24 hrs. After incubation, the non-migrating cells were removed from the upper surface of the membrane and the penetrated cells on the lower surface of the membrane were stained with H.E. Results were plotted as the average number of cells of three random visual fields that migrated through the membrane. (**D**) (right) Effect of *mag-1*-targeted shRNA constructs and scramble control on *mag-1* expression in PLA801D cells. Transfected cells were selected with G418 for 3 weeks until stable clones were obtained and expanded for other experiments. The mRNA and protein level of *mag-1* were assayed using RT-PCR and Western blot. A(left) Adhesion of PLA801D/shRNA and control cells to Matrigel. (**E**) Wound healing migration assay and (**F**) transwell cell invasion assay. The shRNA and scramble control stable transfected cells were cultured and measured using the same methods as mentioned before. Each assay was performed thrice in triplicate. In all studies, statistical significance was determined using One-way ANOVA with non-parametric analysis comparing data points to control. Bars show the standard error of the mean. $*P < 0.05$; $**P < 0.01$.

were screened and identified (Supplementary Figure S1). The EMT6/*mag-1* KD, mock control and scramble-shRNA control (non-silencer) cells were inoculated to the mammary fat pad of female BALB/c mice respectively. The mice were killed when the tumours reached a mean volume of 8 cm^3 and they exhibited a symptom of cachexia. At necropsy, most of the EMT6 mock and EMT6/non-silencer control animals were found to have gross lung nodules that were confirmed to be metastases by histological analysis (Fig. 3A). Although the total tumour volume of each group had no apparent difference, the tumour mass weight of EMT6/*mag-1* KD cells was lighter than that of mock and non-silencer control EMT6 cells, which indicated that *mag-1* may contribute to the construction of tumour parenchyma (Fig. 3B).

Mice bearing EMT6/*mag-1* KD-derived tumours exhibited a significant reduction of lung metastatic foci compared to animals bearing mock or non-silencer control EMT6 cells (Fig. 3C). As far as metastatic frequency was concerned, EMT6/*mag-1* KD cells displayed a depressed ability to form metastatic lung nodules (Fig. 3D). These results demonstrated that the metastatic defect observed in *mag-1* KD EMT6 tumours is due, at least in part, to the absence of *mag-1* in cancer cells.

mag-1 contributes to maintaining the stability of HIF-1α

How does *mag-1* affect the total tumour weight and metastasis? Here, we mimicked the tumour microenvironmental hypoxia condition *in vitro* and found that *mag-1*-stably transfected H1299 cells exhibited an elevated HIF-1α protein level under such condition (Fig. 4A). To determine the role of endogenous *mag-1* in HIF-1α expression, EMT6/*mag-1* KD cells were examined under the same condition with the result of a significantly decreased HIF-1α level compared with the scramble control (Fig. 4B). There was no obvious change in HIF-1α mRNA transcription (Fig. 3B lower two lines). These results indicated that endogenous *mag-1* is an important HIF-1α regulator.

Then we attempted to explore how *mag-1* regulates HIF-1α expression. Interestingly, *mag-1* stably transfected H1299 cells (Fig. 4A and C) as well as African green monkey fibroblast-like cells, COS-7 (Supplementary Figure S2) presented slightly visible HIF-1α expression under normoxia condition indicating that *mag-1* might repress the degradation of HIF-1α under normoxia condition.

Under hypoxia condition, we observed that HIF-1α protein could be detected in both stably transfected *mag-1* and mock control cells after 6 hrs' exposure to hypoxia, and there was no obvious difference in protein levels between the two groups until then. However, the maintenance of HIF-1α seemed a little bit longer in H1299/*mag-1* cells than that in vector control cells (Fig. 4C). After 12 hrs of hypoxia, there was no decline of HIF-1α in H1299/*mag-1* cells compared to its reduction after 10 hrs in H1299 vector cells. The above results suggested that *mag-1* might influence the stability of HIF-1α protein. To address the question, we exposed H1299/*mag-1* cells and vector control to hypoxia for 8 hrs to allow HIF-1α accumulation, then treated them with the protein synthesis inhibitor, cycloheximide, and monitored the rate of HIF-1α decay. We found that HIF-1α half-life in hypoxia increased from 30 min. in the vector control cells to 50 min. in the H1299/*mag-1* cells (Fig. 4D). Collectively, these data showed that *mag-1* is an important determinant of HIF-1α protein stability in cancer cells.

mag-1 potentiates the transcriptional activities of HIF-1α

As HIF-1 is a crucial transcriptional regulator that facilitates cell adaptation to hypoxia, we investigated whether or not the *mag-1*-induced accumulation of HIF-1α is in accordance with an increased transactivational activity monitored carrying out HRE-luciferase reporter assay. Transient overexpression of *mag-1* in H1299 cells resulted in a significant increase in HIF-1α reporter activity in hypoxia as well as in normoxia (Fig. 5A), which conformed to the

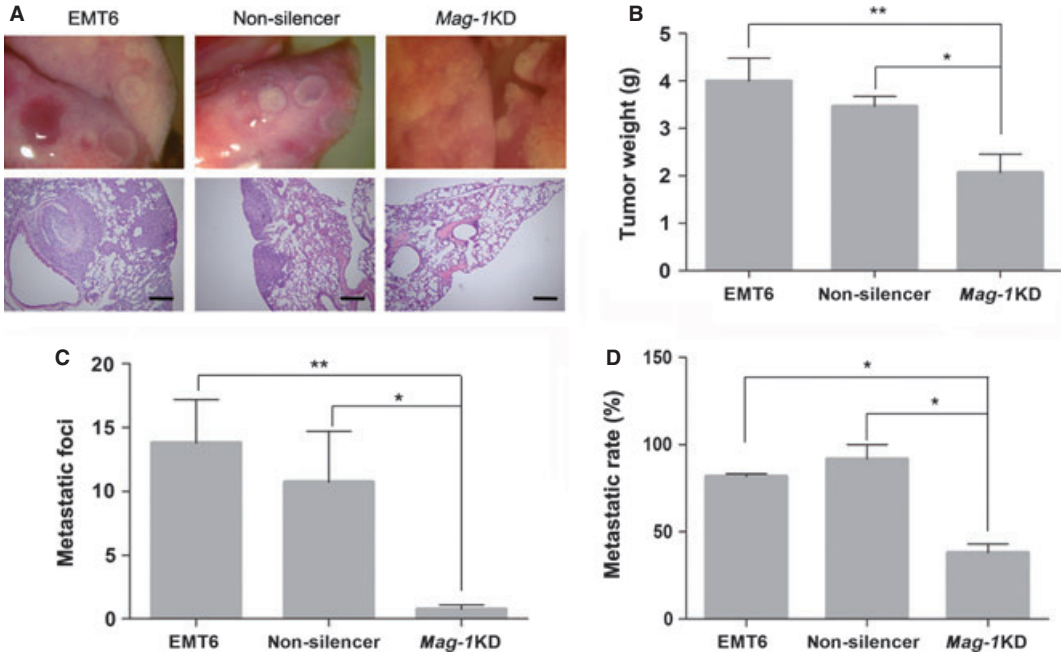

Fig. 3 *mag-1*-silencing defects metastasis of mouse breast cancer EMT6 cells *in vivo*. The EMT6/*mag-1* KD cell strains, mock control and scramble-shRNA control (non-silencer) cells were inoculated to the mammary fat pad of female BALB/c mice respectively. Mice were killed when tumours reached a mean volume of 8 cm^3 and the mice exhibited a symptom of cachexia. (**A**) Photographs of gross and histological representative tumour metastases within lungs arising from EMT6/*mag-1* KD, scramble control and mock control cells. Scale bars represent 50 μm. (**B**) Total weight of tumour mass was measured after mice were dissected. (**C**) The numbers of metastatic foci within the histological specimen of lungs in each group observed and counted under light microscope. (**D**) Metastatic frequency following allograft injection of breast cancer cells. In all studies, statistical significance was determined using One-way ANOVA with non-parametric analysis comparing data points to the scramble or mock control. Bars show the standard error of the mean.*$P < 0.05$; **$P < 0.01$. (Scale bar: 200 μM).

result of elevated HIF-1α expression induced by *mag-1* under both hypoxia and normoxia conditions. H1299 cells transfected with 0.6 μg *mag-1* showed a twofold increase of HRE activity compared to vector control in both normoxia and hypoxia, and the increment of *mag-1* transfectant amount is accompanied by a proportional increase of HRE activity. HIF-1α protein associated with increased HIF-1α activity was confirmed using Western blot (Supplementary Figure S2). The similar result was also observed in COS-7 cells that 0.2 μg *mag-1* transfectant exhibited a 1.5-fold increase of HRE activity in normoxia and 1.75-fold in hypoxia compared to vector control (Fig. 5B). Consistent with the above results, stable transfected H1299/*mag-1* cells also exhibited an elevated HRE activity (Fig. 5C). The induction of HRE activity suggested the activation of HIF-1α transcriptional activity.

The accumulation of HIF-1α was accompanied by an increment expression of HIF-1α protein and translocation to nucleus under hypoxia condition. Under confocal microscope, we observed that HIF-1α expression was elevated significantly in stable transfected H1299/*mag-1* cells compared to that in H1299/vector control cells after 12 hrs exposure to hypoxia. HIF-1α accumulated mainly within the nucleus that contributed to the transcriptional activity (Fig. 5D). Furthermore, the induction of HIF-1 regulating gene, VEGF was evaluated using real time quantitative RT-PCR. Consistent with the elevated HIF-1α activity of H1299/*mag-1* cells, the overexpression of *mag-1* significantly induced the expression in H1299 cells under hypoxia (Fig. 5E). Meanwhile, VEGF significantly downregulating *mag-1* in EMT6 cells could decrease the expression of VEGF both under hypoxia and normoxia conditions (Fig. 5F).

Taken together, we proved that *mag-1* mediates a general effect as an important, oxygen-independent regulator of HIF-1α *via* maintaining its stability, which may contribute to tumour cell's accommodation to tumour microenvironment in both primary and metastatic sites.

mag-1 activates mTOR signalling pathway

As there is an evidence that *mag-1* might play a certain role in tumour cell adaptation to microenvironment, we further probed into the function of *mag-1* in mTOR signal transduction. The results showed that the overexpression of *mag-1* led to a dramatic increase in serum-stimulated endogenous p70S6K1 phosphorylation on Thr389 and 4EBP1 phosphorylation on Thr70 (Fig. 6A). *mag-1* also increased the phosphorylation of exogenous p70S6K1 in PLA801C and human

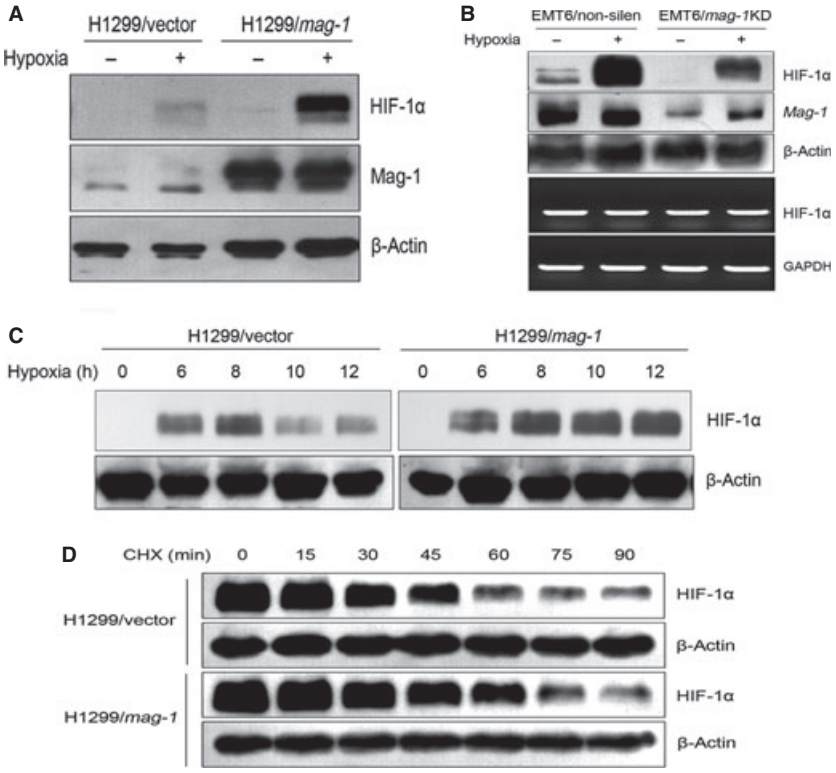

Fig. 4 *mag-1* induces the accumulation of HIF-1α protein under hypoxia. (**A**) H1299 cells stably transfected with *mag-1* or vector were cultivated under normoxia or hypoxia (0.5% O_2) for 12 hrs. HIF-1α protein was detected using Western blot. (**B**) Endogenous *mag-1* was knocked down by specific shRNA in EMT6 cells. EMT6/*mag-1* KD and scramble control cells were subjected to hypoxia for 12 hrs. Protein accumulation of HIF-1α was analysed using Western blot (upper two lines), whereas the corresponding mRNA levels of HIF-1α were assessed using RT-PCR (lower two lines). (**C**) H1299/*mag-1* and vector control cells were subjected to hypoxia for the indicated time. The induction of *mag-1* expression was analysed using Western blot. (**D**) Effects of *mag-1* overexpression on HIF-1α half-life. *mag-1*-stably transfected H1299 and mock control cells were incubated in hypoxia for 8 hrs and then treated with 25 g/ml cycloheximide, after which the decay of HIF-1α was monitored at the indicated times using Western blot.

embryonic kidney cells, HEK293T (Fig. 6B). Given that both p70S6K1 and 4EBP1 are two specific effectors of mTOR activation, we examined the effect of rapamycin, a specific inhibitor of mTOR activation, on the increased S6K1 and 4EBP-1 phosphorylation in PLA801C and HEK293T cells with overexpressed *mag-1*. As is shown in Figure 5A and B, the serum-stimulated phosphorylation of p70S6K1-T389 and 4EBP1-T70 was completely blocked in the presence of rapamycin in both PLA801C/*mag-1* and HEK293/*mag-1* cells. There was no significant difference in the phosphorylation of Akt between control and *mag-1*-overexpressing cells (Fig. 6A and B), indicating that the overexpression of *mag-1* led to direct activation of mTOR pathway, but had no influence on upstream PI3K/AKT pathway. Accordingly, when we down-regulated the endogenous *mag-1* expression of PLA801D, the phosphorylation of S6K1 and 4EBP-1 phosphorylation reduced in PLA801D/*mag-1* KD cells. Meanwhile, the level of phosphorylated Akt showed no difference between control and *mag-1* knocked-down cells (Fig. 6C).

As HIF-1α protein itself is a downstream target of mTOR, we further detected the effect of mTOR inhibition by rapamycin on *mag-1*-mediated HIF-1α accumulation. Figure 6D indicated that HIF-1α significantly declined in H1299/*mag-1* cells after the rapamycin treatment either under hypoxia or normoxia condition. The above data suggested that *mag-1* as a signalling regulator in the activation of mTOR pathway contributes to the accumulation of HIF-1α.

mag-1-mediated mTOR signalling is required for metastasis

To further examine whether or not *mag-1* promoted cancer metastasis *via* activating mTOR signalling pathway, PLA801C/*mag-1* cells were treated or left untreated by 20 nM rapamycin for 24 hrs prior to cytological analysis. As is shown in Figure 7A, the addition of rapamycin reduced the elevated cell migration of PLA801C/*mag-1* cells across the injury line during the follow-up period of 20 hrs (compared to the untreated cells, $P < 0.01$). The rapamycin treatment also made significant change of cell migration in mock control cells. Cell

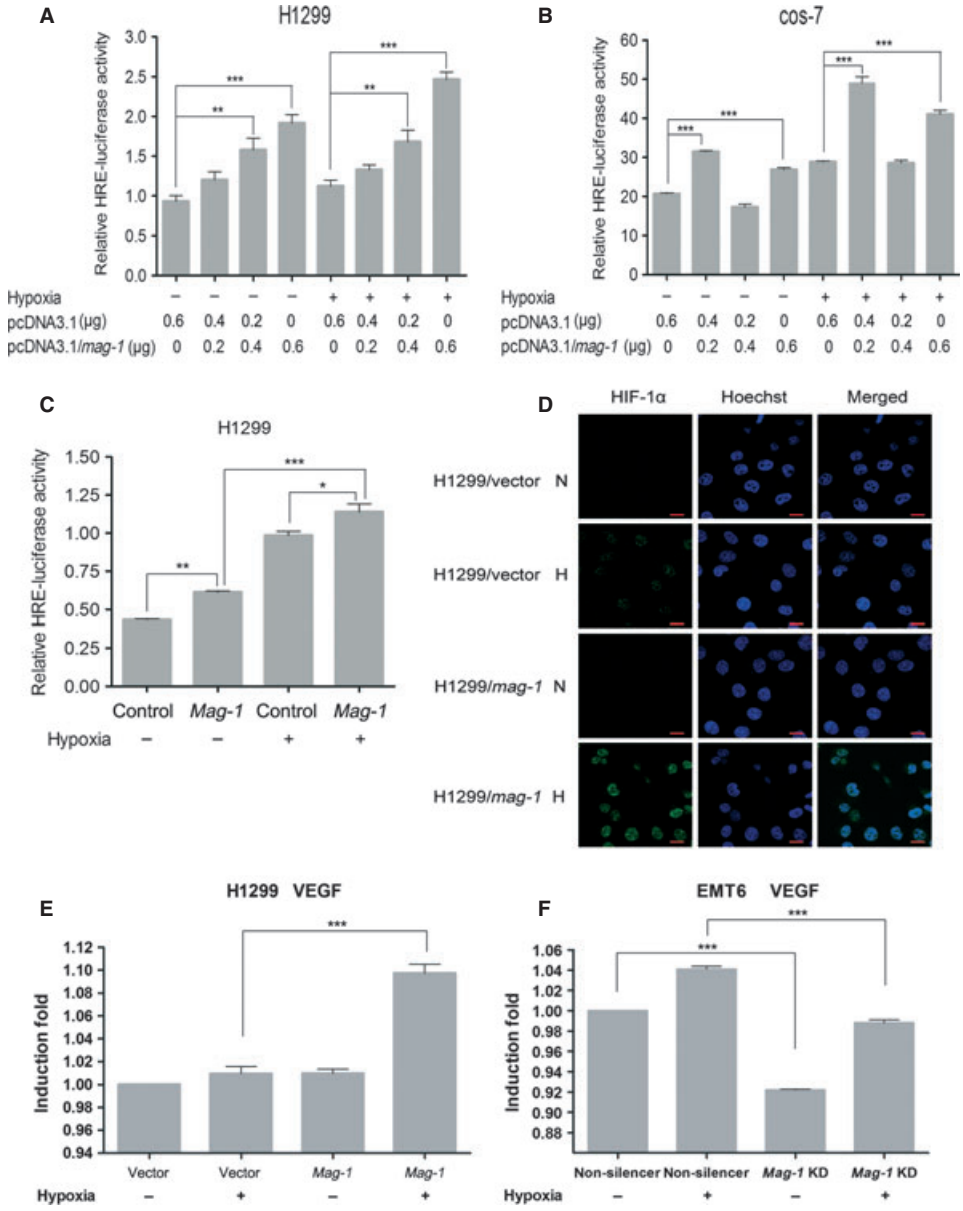

Fig. 5 *mag-1* potentiates the transcriptional activity of HIF-1α under hypoxia. (**A**) and (**B**) H1299 cells and COS-7 cells were plated 18 hrs before transfection by Mega Tran 1.0 (Origene) according to the manufacturer's instructions. The following plasmids were co-transfected into cells: 500 ng HRE-Luc in combination with 0.5 ng of the Renilla internal control CMV-pRNL (Promega, Madison, WI, USA), and 0.2, 0.4 or 0.6 μg pcDNA3.1/*mag-1*. After transfection, cells were cultured 6–10 hrs under hypoxia or normoxia conditions. The total amount of DNA transfected was adjusted to 0.6 μg with pcDNA3.1 (mock). (**C**) Stably transfected H1299/*mag-1* cells and mock control were transfected only with HRE-Luc Luciferase and Renilla internal control plasmids. Luciferase activities were measured 24–36 hrs after hypoxia using the Dual-luciferase reporter system according to the manufacturer's protocol (Promega). The ratio of Firefly/Renilla luciferase activity was determined in relative light units (RLU). The data shown are from a representative experiment performed in triplicate. Bars show the standard error of the mean. Statistical significance was determined using One-way ANOVA with non-parametric analysis comparing data points to the scramble or mock control. $^{**}P < 0.01$; $^{***}P < 0.001$. (**D**) Comparison of HIF-1α expression between H1299/*mag-1* and H1299/vector control cells under normoxia condition or exposure to hypoxia for 12 hrs using immunofluorescent staining. The representative results were observed and photographed under Zeiss Confocal laser-scanning microscope. Scale bars represent 20 μm. (**E**) and (**F**) Real time PCR analysis were performed in triplicate in three independent experiments to confirm the effect of manipulating the expression of *mag-1* gene on HIF-1-induced VEGF mRNA expression in H1299 (E) and EMT6 (F) cells under normoxia and hypoxia conditions. GAPDH was used to normalize the quantitative real time PCR results. The results are presented as bar graphs showing the means ± S.D.

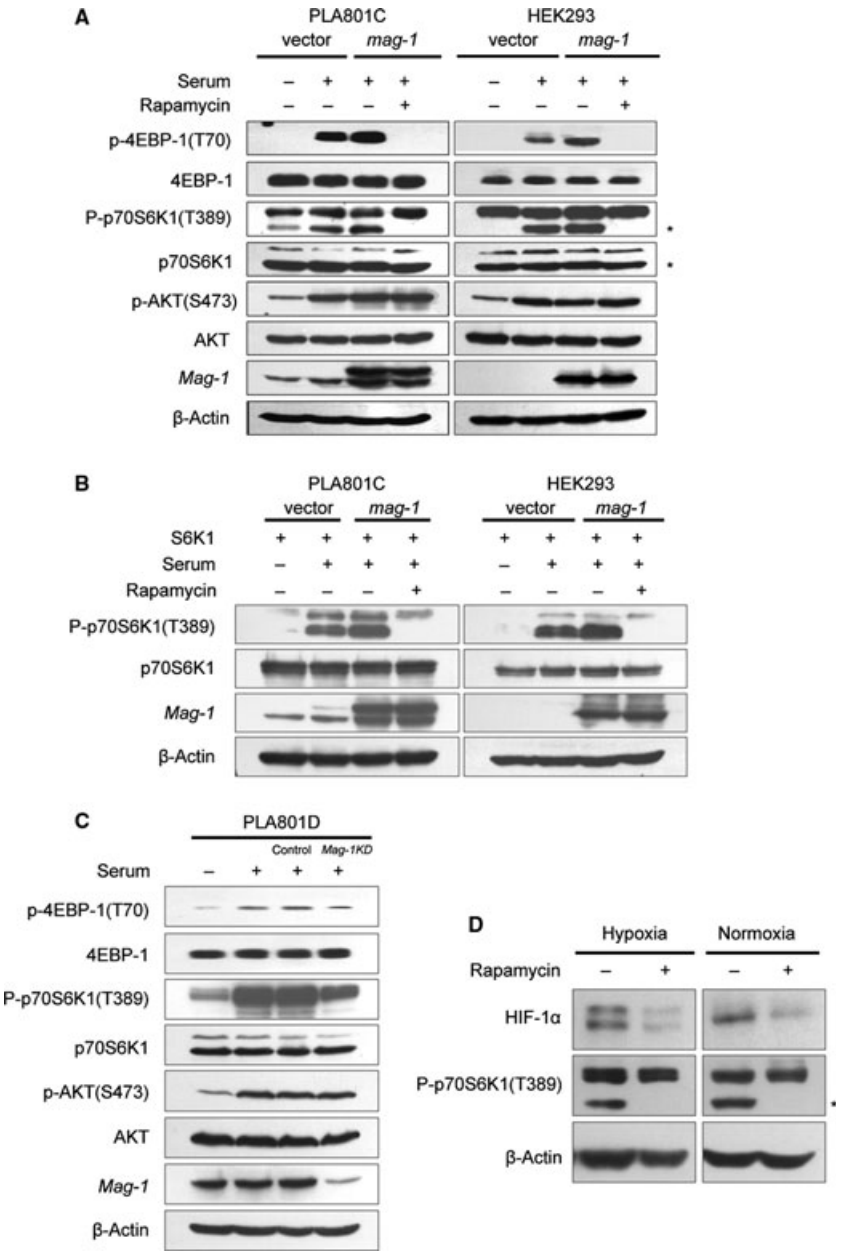

Fig. 6 *mag-1* induces activation of mTOR signalling transduction pathway. (**A**) HEK293 and PLA801C cells were transfected with pcDNA3.1/*mag-1* and control vector for about 12 hrs followed by serum starvation for 24 hrs and then stimulated with 10% foetal bovine serum for 20 min. prior to cell lysis. For inhibitory assay, cells were treated with 20 nM rapamycin 30 min. before serum stimulation. The levels of regulators in PI3K/AKT/mTOR signalling pathways were detected using Western blot using the antibodies shown to the left of the panels. (**B**) PLA801C and HEK293 cells were co-transfected with pcDNA3.1/*mag-1* and pcDNA3.1/S6K1 plasmids followed by the treatment as mentioned above. The phosphorylation of exogenous p70S6K1 (T389) was analysed using Western blot. (**C**) PLA801D cells stably transfected with *mag-1*/shRNA or scramble control shRNA were cultured with serum-free medium for 24 hrs and then stimulated with 10% foetal bovine serum for 20 min. prior to cell lysis. The phosphorylation of p70S6K1 (T389), 4EBP-1(T70) and AKT (S473) were analysed using Western blot using the specific antibodies respectively. (**D**) H1299/*mag-1* cells were exposure to hypoxia for 8 hrs or under normoxia, followed by 20 nM rapamycin treatment for 1 hr prior to cell lysis. The level of HIF-1α and phosphorylation of p70S6K1 (T389) was analysed using Western blot. The line of β-Actin indicated the equal loading as an internal control.

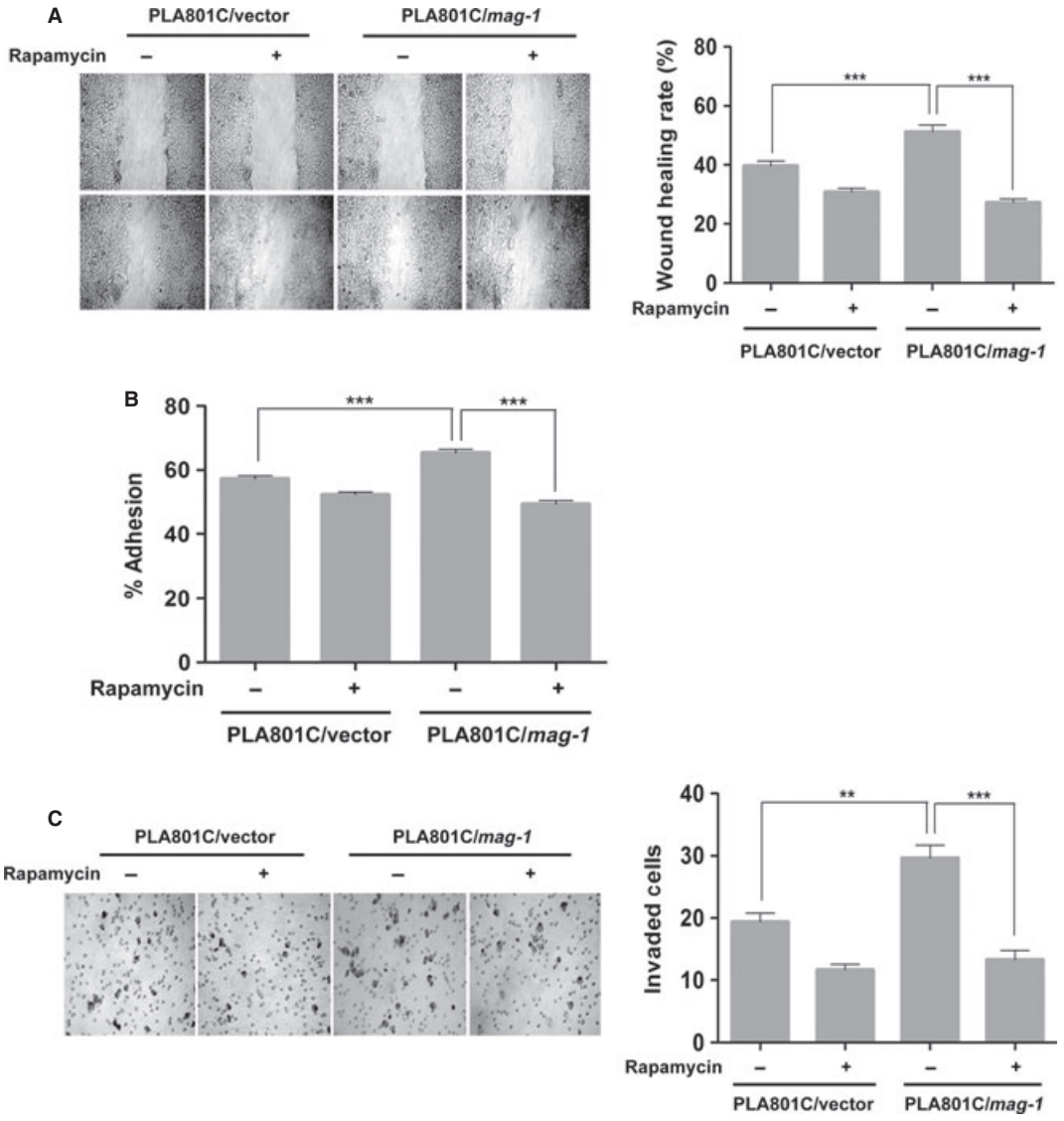

Fig. 7 Effect of *mag-1* on tumour metastasis was significantly interrupted by mTOR inhibitor, rapamycin *in vitro*. (**A**) Effect of rapamycin on cell migration of PLA801C/*mag-1* and mock control cells. Stably transfected PLA801C/*mag-1* cells were treated or left untreated with 20 nM rapamycin for 12 hrs, and then subjected to wound healing assay. Representative photographs of wound closure monitored under microscope are shown and the wound healing rate was calculated as indicated in experimental procedures. (**B**) Effect of rapamycin on adhesion of PLA801C/*mag-1* and mock control cells to Matrigel. Cells were pretreated or not by 20 nM rapamycin for 24 hrs, and then plated in the microwells coated with Matrigel. The detailed method is as mentioned previously. (**C**) Effect of rapamycin on cell invasion through Matrigel-coated transwell. Cells were pretreated or not by 20 nM rapamycin for 24 hrs, and then plated in the Matrigel-coated upper microwells of transwell. Each assay was performed thrice in triplicate. Bars show the standard error of the mean. Statistical significance was determined using One-way ANOVA with non-parametric analysis comparing data points to the scramble or mock control. $^{**}P < 0.01$; $^{***}P < 0.001$.

adhesion assay revealed that rapamycin abolished the increased cell migration of PLA801C/*mag-1* cells to Matrigel, which was in contrast with the untreated cells ($P < 0.001$; Fig. 7B). Furthermore, inhibition of mTOR signalling pathway by rapamycin depressed the invasion capability of PLA801C/*mag-1* cells compared to the untreated cells ($P < 0.001$; Fig. 7C). Collectively, these results provided the evidence that mTOR signalling activation played a central role in *mag-1* regulating metastasis of lung cancer cells, and the disruption mTOR signalling might significantly prohibit the metastatic promotion function of *mag-1*.

Discussion

Tumour microenvironment is heterogeneous as a result of the deficiency vasculature and the out-of- control growth of cancer cells. The majority of malignant solid tumours have been found to prosper under the microenvironment of low oxygen tension or hypoxia [38, 39]. Tissue hypoxia significantly contributes to tumour invasion and metastasis by the mechanisms of altering malignant cell mobility, migration, invasiveness and angiogenesis [40]. In turn, tumour cells establish a specific accommodation system, such as genetic instability, aerobic glycolysis, abnormal apoptotic signals and loss of cell cycle control, fostering tumour progression and metastasis [41]. Cancer cells initiate hypoxia response by manipulating the master switch regulators and stimulating the expression of several genes responsible for the survival and metastasis of tumour cells. Moreover, cancer cells actively perform 'metabolic reprogramming' mechanism to reinforce the nutritional and energy supply, promoting tumour progression and aggressive dissemination [42–44]. Therefore, it is a critical priority to identify the key regulators that contribute to the development of tumour microenvironmental adaptation mechanisms.

In this study, we have identified unique roles of the metastasis-associated gene *mag-1* which presents dual functions in regulating hypoxia and metabolism, the two important aspects in microenvironmental adaptation. HIF-1α is the master transcriptional regulator that facilitates cellular adaptation to low oxygen availability [45]. Here, we showed that *mag-1* influences significant accumulation of HIF-1α under hypoxia condition. HIF-1α is targeted for degradation by prolyl hydroxylases (PHD), resulting in ubiquitination by VHL ubiquitin ligase and degradation by the proteosomal pathway [46, 47]. Under hypoxia condition, PHD was suppressed, leading to HIF-1a protein stabilization. Thus, *mag-1* might interfere with the degradation of HIF-1α and mediate its accumulation. On the other hand, *mag-1* also induces HIF-1α transcriptional activity, which contributes to the elevation of VEGF expression to develop neovasculature and glycolytic metabolic shift by inducing the expression of genes encoding glucose transporters (Glut1) to provide glucose supply.

It is worth mentioning that *mag-1* can stabilize HIF-1α protein in normoxia. In fact, there are some related reports demonstrating the regulation of HIF-1α protein under normoxia condition. Immunohistochemical examination of brain, kidney, liver, heart and skeletal muscle reveals that HIF-1α appears in the mice living under normoxic condition and increases further in response to systemic hypoxia [48]. Some molecules were proved to induce the increase of HIF-1α protein in normoxia. It is reported that interleukin-1β normoxic induction of HIF-1α can be performed by involving the extracellular signal-regulated kinase 1/2 pathway in normal human cytotrophoblast cells [49]. In addition, Nitric oxide is another effector that impairs normoxic degradation of HIF-1α by the inhibition of prolyl hydroxylases [50]. Further detailed investigation into the mechanism of *mag-1*- induced stabilization HIF-1α will be valuable to unveil the function of *mag-1* in tumour microenvironmental adaptation and metastasis.

Moreover, *mag-1* was also demonstrated as a potent activator of mTOR signalling pathway, promoting protein synthesis by the phosphorylation of p70S6K1 and 4EBP1. The application of rapamycin could suppress *mag-1*-induced mTOR activation accompanied by the inhibition of increased cell migration, adhesion and invasion. Notably, HIF-1α protein itself is a downstream target of mTOR which contributes to oxygen-independent regulation of HIF-1α [18, 51–53]. HIF-1α protein expression and the related activity can also be slightly increased by *mag-1* under normoxia, indicating the accumulation of HIF-1α protein, at least in part might result from *mag-1*-induced mTOR pathway activation. In this regard, *mag-1* integrates its function by regulating mTOR pathway with the stabilization HIF-1α, and the underlying mechanisms deserve to be explored. Together, these proofs demonstrate that *mag-1* makes cancer cells prone to adapting tumour microenvironment during their progression and metastasis. Naturally, if we cause knockdown, the endogenous *mag-1*, the intrinsic metabolism and cellular reaction against hypoxia will be interrupted, resulting in the decline of total tumour weight and the numbers of decreased metastatic nodules *in vivo*.

During the study on *mag-1* in progress, a novel human LPAAT isozyme, LPAAT-θ was cloned by Tang *et al.* that shares 100% identity with *mag-1*, whereas its function has not been clarified yet [30]. Later that year, the same sequence was reported as a microsomal acyl-CoA: glycerol-3-phosphate acyltransferase, GPAT3, which is a major contributor to GPAT activity in 3T3-L1 adipocytes [33], and also found to be regulated by insulin-stimulated phosphorylation and plays a distinct role in adipogenesis [32]. Recently, Sukumaran *et al.* showed that the same cDNA has only AGPAT activity instead of the GPAT activity in HEK293 cells. Until now, there has been no reasonable explanation of the discrepancy of two distinct enzymatic activities presented by the same cDNA sequence. Which *mag-1* enzymatic activity possesses tumour metastatic cascades and whether this lipid biogenesis activity is necessary for manipulating metastasis is worthwhile to determine in the future work.

In conclusion, our findings that *mag-1* is indispensable to tumour metastasis *via* dual regulation mechanism in tumour microenvironment suggest that the intervention in its function has valuable implications for the treatment of metastatic disease.

Acknowledgements

We are grateful to Prof. EE Voest (University Medical Center Utrecht, The Netherlands) for providing the HRE-luciferase reporter constructs and Prof. Jie Chen for providing pcDNA3.1/p70S6K1 plasmid (Illinois University, USA). We thank Professor Lingling Zhu for her help with hypoxia experiments. This work was supported by grants from Chinese National Natural Science Foundation (30800418, 30470389, 30570800 and 30970742) and Chinese State Key Projects for Basic Research (2002CB513105, 2009CB552104, and 2012CB518200).

Conflict of interest

The authors confirm that there are no conflicts of interest.

Supporting information

Additional Supporting Information may be found in the online version of this article:

Data S1 Materials and methods.

Fig S1 Analyzing the interference efficiency of stable clones transfected with *mag-1*-targeted shRNA in mouse breast cancer EMT6 cells.

Fig S2 Analyzing the transfection efficiency and induction of HIF-1α in hypoxia. H1299 cells and COS-7 cells were plated for 18 hrs before transfected by Mega Tran 1.0 (OriGene) according to the manufacturer's instructions.

Please note: Wiley-Blackwell are not responsible for the content or functionality of any supporting materials supplied by the authors. Any queries (other than missing material) should be directed to the corresponding author for the article.

References

1. **Friedman A, Kim Y.** Tumor cells proliferation and migration under the influence of their microenvironment. *Math Biosci Eng*. 2011; 8: 371–83.
2. **Finger EC, Giaccia AJ.** Hypoxia, inflammation, and the tumor microenvironment in metastatic disease. *Cancer Metastasis Rev*. 2010; 29: 285–93.
3. **Booth BW, Boulanger CA, Anderson LH, *et al.*** The normal mammary microenvironment suppresses the tumorigenic phenotype of mouse mammary tumor virus-neu-transformed mammary tumor cells. *Oncogene*. 2011; 30: 679–89.
4. **Bristow RG, Hill RP.** Hypoxia and metabolism. Hypoxia, DNA repair and genetic instability. *Nat Rev Cancer*. 2008; 8: 180–92.
5. **Jin S, DiPaola RS, Mathew R, *et al.*** Metabolic catastrophe as a means to cancer cell death. *J Cell Sci*. 2007; 120: 379–83.
6. **Acker T, Plate KH.** Hypoxia and hypoxia inducible factors (HIF) as important regulators of tumor physiology. *Cancer Treat Res*. 2004; 117: 219–48.
7. **Salceda S, Caro J.** Hypoxia-inducible factor 1alpha (HIF-1alpha) protein is rapidly degraded by the ubiquitin-proteasome system under normoxic conditions. Its stabilization by hypoxia depends on redox-induced changes. *J Biol Chem*. 1997; 272: 22642–7.
8. **Semenza GL.** HIF-1, O(2), and the 3 PHDs: how animal cells signal hypoxia to the nucleus. *Cell*. 2001; 107: 1–3.
9. **Jewell UR, Kvietikova I, Scheid A, *et al.*** Induction of HIF-1alpha in response to hypoxia is instantaneous. *FASEB J*. 2001; 15: 1312–4.
10. **Ema M, Hirota K, Mimura J, *et al.*** Molecular mechanisms of transcription activation by HLF and HIF1alpha in response to hypoxia: their stabilization and redox signal-induced interaction with CBP/p300. *EMBO J*. 1999; 18: 1905–14.
11. **Jiang BH, Rue E, Wang GL, *et al.*** Dimerization, DNA binding, and transactivation properties of hypoxia-inducible factor 1. *J Biol Chem*. 1996; 271: 17771–8.
12. **Dames SA, Martinez-Yamout M, De Guzman RN, *et al.*** Structural basis for Hif-1 alpha/CBP recognition in the cellular hypoxic response. *Proc Natl Acad Sci USA*. 2002; 99: 5271–6.
13. **Semenza GL.** Evaluation of HIF-1 inhibitors as anticancer agents. *Drug Discov Today*. 2007; 12: 853–9.
14. **Semenza GL.** HIF-1 inhibitors for cancer therapy: from gene expression to drug discovery. *Curr Pharm Des*. 2009; 15: 3839–43.
15. **Katsuta M, Miyashita M, Makino H, *et al.*** Correlation of hypoxia inducible factor-1alpha with lymphatic metastasis via vascular endothelial growth factor-C in human esophageal cancer. *Exp Mol Pathol*. 2005; 78: 123–30.
16. **Liao D, Corle C, Seagroves TN, *et al.*** Hypoxia-inducible factor-1alpha is a key regulator of metastasis in a transgenic model of cancer initiation and progression. *Cancer Res*. 2007; 67: 563–72.
17. **Lu X, Yan CH, Yuan M, *et al.*** *In vivo* dynamics and distinct functions of hypoxia in primary tumor growth and organotropic metastasis of breast cancer. *Cancer Res*. 2010; 70: 3905–14.
18. **Wouters BG, Koritzinsky M.** Hypoxia signalling through mTOR and the unfolded protein response in cancer. *Nat Rev Cancer*. 2008; 8: 851–64.
19. **Zhou H, Huang S.** Role of mTOR signaling in tumor cell motility, invasion and metastasis. *Curr Protein Pept Sci*. 2011; 12: 30–42.
20. **Chen JS, Wang Q, Fu XH, *et al.*** Involvement of PI3K/PTEN/AKT/mTOR pathway in invasion and metastasis in hepatocellular carcinoma: association with MMP-9. *Hepatol Res*. 2009; 39: 177–86.
21. **Shaw RJ, Cantley LC.** Ras, PI(3)K and mTOR signalling controls tumour cell growth. *Nature*. 2006; 441: 424–30.
22. **Hay N, Sonenberg N.** Upstream and downstream of mTOR. *Genes Dev*. 2004; 18: 1926–45.
23. **Shahbazian D, Roux PP, Mieulet V, *et al.*** The mTOR/PI3K and MAPK pathways converge on eIF4B to control its phosphorylation and activity. *EMBO J*. 2006; 25: 2781–91.
24. **Roccaro AM, Sacco A, Husu EN, *et al.*** Dual targeting of the PI3K/Akt/mTOR pathway as an antitumor strategy in Waldenstrom macroglobulinemia. *Blood*. 2010; 115: 559–69.
25. **Easton JB, Houghton PJ.** mTOR and cancer therapy. *Oncogene*. 2006; 25: 6436–46.
26. **Seeliger H, Guba M, Kleespies A, *et al.*** Role of mTOR in solid tumor systems: a therapeutical target against primary tumor growth, metastases, and angiogenesis. *Cancer Metastasis Rev*. 2007; 26: 611–21.
27. **Jiang Y, Zhang W, Kondo K, *et al.*** Gene expression profiling in a renal cell carcinoma cell line: dissecting VHL and hypoxia-dependent pathways. *Mol Cancer Res*. 2003; 1: 453–62.
28. **Zhang J, Meng Y, Lin H, *et al.*** [Promotion of MAG-1 on Metastasis of Lung Cancer Cells *in vitro* and Its Expression in Lung Cancer Tissue of 24 Cases.]. *Zhongguo Fei Ai Za Zhi*. 2009; 12: 93–9.
29. **Yamada S, Ohira M, Horie H, *et al.*** Expression profiling and differential screening between hepatoblastomas and the corresponding normal livers: identification of high expression of the PLK1 oncogene as a poor-prognostic indicator of hepatoblastomas. *Oncogene*. 2004; 23: 5901–11.
30. **Tang W, Yuan J, Chen X, *et al.*** Identification of a novel human lysophosphatidic acid acyltransferase, LPAAT-theta, which activates mTOR pathway. *J Biochem Mol Biol*. 2006; 39: 626–35.
31. **Gimeno RE, Cao J.** Thematic review series: glycerolipids. Mammalian glycerol-3-phosphate acyltransferases: new genes for an old activity. *J Lipid Res*. 2008; 49: 2079–88.

32. **Shan D, Li J, Wu L, *et al.*** GPAT3 and GPAT4 are regulated by insulin-stimulated phosphorylation and play distinct roles in adipogenesis [S]. *J Lipid Res*. 2010; 51: 1971–81.
33. **Cao J, Li JL, Li D, *et al.*** Molecular identification of microsomal acyl-CoA:glycerol-3-phosphate acyltransferase, a key enzyme in de novo triacylglycerol synthesis. *Proc Natl Acad Sci USA*. 2006; 103: 19695–700.
34. **Sukumaran S, Barnes RI, Garg A, *et al.*** Functional characterization of the human 1-acylglycerol-3-phosphate-O-acyltransferase isoform 10/glycerol-3-phosphate acyltransferase isoform 3. *J Mol Endocrinol*. 2009; 42: 469–78.
35. **Koh MY, Darnay BG, Powis G.** Hypoxia-associated factor, a novel E3-ubiquitin ligase, binds and ubiquitinates hypoxia-inducible factor 1alpha, leading to its oxygen-independent degradation. *Mol Cell Biol*. 2008; 28: 7081–95.
36. **Giles RH, Lolkema MP, Snijckers CM, *et al.*** Interplay between VHL/HIF1alpha and Wnt/beta-catenin pathways during colorectal tumorigenesis. *Oncogene*. 2006; 25: 3065–70.
37. **Jiang D, Ying W, Lu Y, *et al.*** Identification of metastasis-associated proteins by proteomic analysis and functional exploration of interleukin-18 in metastasis. *Proteomics*. 2003; 3: 724–37.
38. **Greco O, Scott S.** Tumor hypoxia and targeted gene therapy. *Int Rev Cytol*. 2007; 257: 181–212.
39. **Chan N, Milosevic M, Bristow RG.** Tumor hypoxia, DNA repair and prostate cancer progression: new targets and new therapies. *Future Oncol*. 2007; 3: 329–41.
40. **Holmquist-Mengelbier L, Fredlund E, Lofstedt T, *et al.*** Recruitment of HIF-1alpha and HIF-2alpha to common target genes is differentially regulated in neuroblastoma: HIF-2alpha promotes an aggressive phenotype. *Cancer Cell*. 2006; 10: 413–23.
41. **Carlini MJ, De Lorenzo MS, Puricelli L.** Cross-talk between Tumor Cells and the Microenvironment at the Metastatic Niche. *Curr Pharm Biotechnol*. 2011; 12: 1900–8.
42. **Chiche J, Brahimi-Horn MC, Pouyssegur J.** Tumour hypoxia induces a metabolic shift causing acidosis: a common feature in cancer. *J Cell Mol Med*. 2010; 14: 771–94.
43. **Semenza GL.** Regulation of cancer cell metabolism by hypoxia-inducible factor 1. *Semin Cancer Biol*. 2009; 19: 12–6.
44. **Vaupel P.** Metabolic microenvironment of tumor cells: a key factor in malignant progression. *Exp Oncol*. 2010; 32: 125–7.
45. **Semenza GL.** Targeting HIF-1 for cancer therapy. *Nat Rev Cancer*. 2003; 3: 721–32.
46. **Jaakkola P, Mole DR, Tian YM, *et al.*** Targeting of HIF-alpha to the von Hippel-Lindau ubiquitylation complex by O2-regulated prolyl hydroxylation. *Science*. 2001; 292: 468–72.
47. **Ivan M, Kondo K, Yang H, *et al.*** HIFalpha targeted for VHL-mediated destruction by proline hydroxylation: implications for O2 sensing. *Science*. 2001; 292: 464–8.
48. **Stroka DM, Burkhardt T, Desbaillets I, *et al.*** HIF-1 is expressed in normoxic tissue and displays an organ-specific regulation under systemic hypoxia. *FASEB J*. 2001; 15: 2445–53.
49. **Qian D, Lin HY, Wang HM, *et al.*** Normoxic induction of the hypoxic-inducible factor-1 alpha by interleukin-1 beta involves the extracellular signal-regulated kinase 1/2 pathway in normal human cytotrophoblast cells. *Biol Reprod*. 2004; 70: 1822–7.
50. **Metzen E, Zhou J, Jelkmann W, *et al.*** Nitric oxide impairs normoxic degradation of HIF-1alpha by inhibition of prolyl hydroxylases. *Mol Biol Cell*. 2003; 14: 3470–81.
51. **Garcia-Maceira P, Mateo J.** Silibinin inhibits hypoxia-inducible factor-1alpha and mTOR/p70S6K/4E-BP1 signalling pathway in human cervical and hepatoma cancer cells: implications for anticancer therapy. *Oncogene*. 2009; 28: 313–24.
52. **Li W, Petrimpol M, Molle KD, *et al.*** Hypoxia-induced endothelial proliferation requires both mTORC1 and mTORC2. *Circ Res*. 2007; 100: 79–87.
53. **Land SC, Tee AR.** Hypoxia-inducible factor 1alpha is regulated by the mammalian target of rapamycin (mTOR) via an mTOR signaling motif. *J Biol Chem*. 2007; 282: 20534–43.